Structural vs. compositional disorder in thermal conductivity reduction of SiGe alloys

Jihui Nie, Raghavan Ranganathan, Zhi Liang, and Pawel Keblinski

Citation: Journal of Applied Physics **122**, 045104 (2017); doi: 10.1063/1.4994169
View online: https://doi.org/10.1063/1.4994169
View Table of Contents: http://aip.scitation.org/toc/jap/122/4
Published by the American Institute of Physics

Structural vs. compositional disorder in thermal conductivity reduction of SiGe alloys

Jihui Nie, Raghavan Ranganathan, Zhi Liang, and Pawel Keblinski
Department of Materials Science and Engineering, Rensselaer Polytechnic Institute, Troy, New York 12180, USA

(Received 29 May 2017; accepted 4 July 2017; published online 26 July 2017)

We use equilibrium molecular dynamics simulations to determine the relative role of compositional and structural disorder in a phononic thermal conductivity reduction by studying three 50-50 SiGe alloy structures: ordered alloys, disordered alloys, and amorphous alloys, as well as pure amorphous Si and Ge structures for reference. While both types of disorders significantly reduce thermal conductivity, structural disorder is much more effective to this aim. The examination of phonon lifetimes in disordered alloys shows high values in a low frequency regime governed by Umklapp scattering that are reduced rapidly with increasing frequency following Rayleigh scattering behavior. The local properties analysis reveals that the structural disorder leads to elastic heterogeneities that are significantly larger than density heterogeneities, which is likely the key reason for amorphous semiconductor alloys having lower thermal conductivity than disordered alloys. Temperature dependence of thermal conductivity indicates the importance of propagating phonons and associated Umklapp scattering in SiGe alloy structures. Interestingly, longitudinal modes in amorphous and disordered alloys exhibit similar lifetimes, while transverse modes lifetimes show significant differences and are more temperature dependent. *Published by AIP Publishing.* [http://dx.doi.org/10.1063/1.4994169]

I. INTRODUCTION

Semiconducting and insulating alloys are of interest for many applications, including thermoelectric converters[1] and thermal barrier coatings,[2] where low thermal conductivity plays an important role. Alloying[3,4] and nanostructuring[5–8] have been proposed as the main methods to reduce thermal conductivity. Alloying is demonstrated to effectively scatter the high-frequency phonons by compositional disorder.[4] Nanostructuring to forms of nanowires,[5] nanoporous structures,[6] nanocomposites,[7] and superlattices[8] can scatter the lower frequency phonons.

Numerous studies have been carried out to investigate the thermal conductivity of SiGe alloys. A dramatic decrease in the thermal conductivity is present with small concentration of Ge added to Si, observed in both experiments and simulations.[9–11] The mass disorder was demonstrated to be dominant in phonon scattering in the SiGe alloy, while bond disorder and strain effects play a minor role.[4,12] A recent study shows SiGe nanostructures, including thin film, superlattices and nanocomposites, exhibit even lower thermal conductivity than bulk alloys, and almost reach the amorphous limit.[13] The thermal transport in SiGe nanostructures is tunable by thickness (thin films), periodic thickness (superlattices), and grain size (nanocomposites) through boundary scattering.[13] A study on amorphous SiGe suggests that the reduction of thermal conductivity may be attributed to a wide spread in the mean free path of phonons dominating the thermal transport, related to enhanced phonon-phonon scattering.[14]

However, the underlying phonon transport and scattering mechanism are still unclear. In this paper, we present molecular dynamics (MD) simulations aimed at characterizing the relative role of two types of atomic disorders in heat transport, namely, compositional disorder and structural disorder in semiconductor alloys. The compositional disorder arises from the non-regular placement of two or more atomic species on a crystalline lattice, while in the case of most severe structural disorder, the lattice is not present at all and the structure is amorphous. Previous extensive work on this topic[15–17] was done for alloys where interatomic interactions were described by a pair Lennard–Jones (LJ) potential, typically used to model metallic alloys (we will refer to them as LJ alloys). The alloys modeled by LJ potential are characterized by relatively large anharmonicity and relatively dense-packed structures, while the model semiconductor SiGe alloys presented in this work are much more harmonic, and represent low-coordination, open network structures. As we will show, this leads to a significant role of low-frequency phonons in thermal transport and strong temperature effects exhibited not only by ordered structures, but also by disordered SiGe alloys.

The sample preparation and simulation details are described in Sec. II. The results and discussion on the thermal conductivity, phonon lifetime analysis, local property analysis, and temperature dependence are presented in Sec. III, followed by the conclusions in Sec. IV.

II. SIMULATION METHODOLOGY

A. Model structures

To expose the relative role of each type of disorder in semiconductor alloys, we study the thermal conductivities, phonon lifetimes, local densities, and local elastic constants of different model SiGe 50–50 alloy structures (see Fig. 1). The first structure is the reference ordered structure (o-SiGe), which has a CuAu-I-type crystal structure and has been observed experimentally by Tischler *et al.*[18] The

disordered structure (d-SiGe) is a random 50–50 alloy, where Si and Ge atoms are placed randomly on the diamond cubic crystal structure. The a-SiGe alloy was prepared by melting the d-SiGe structure at 3500 K and continuously quenching to 300 K with a quench rate of 1×10^{12} K/s at zero external pressure.[19] Using a similar protocol, we prepared pure amorphous silicon (a-Si) and pure amorphous germanium (a-Ge) structures for reference.

All structures were confined to cubic simulation cells and their dimensions vary from 4 to 30 cubic unit cells of the original crystal structure, resulting in 512 to 216 000 atoms in total.

B. Force field and thermal conductivity determination

In all simulations, the interaction between Si and Ge atoms is described by the Tersoff empirical potential.[20] This potential is fitted to the pure Si and Ge lattice constants of 5.431 Å and 5.658 Å, respectively.[21] Skye and Schelling[12] have demonstrated that the lattice constant of Si_xGe_{1-x} alloys closely follows Vegard's law (arithmetic mean of constituent values). Thus, we set the initial lattice constant of the SiGe alloy as 5.545 Å, and relax all alloy structures at a constant temperature of 300 K and zero external pressure for 50 ps.

Such equilibrated structures were evolved at constant energy and volume (NVE) from 4 ns to 10 ns depending on the structure type and size, during which we monitored the fluctuating heat current, $J(t)$. We then calculated the thermal conductivity from the integral of heat current autocorrelation function, using the Green–Kubo relation based on the fluctuation-dissipation theorem[22]

$$\kappa(\tau_m) = \frac{1}{Vk_BT^2}\int_0^{\tau_m} \langle J(\tau)\cdot J(0)\rangle d\tau, \quad (1)$$

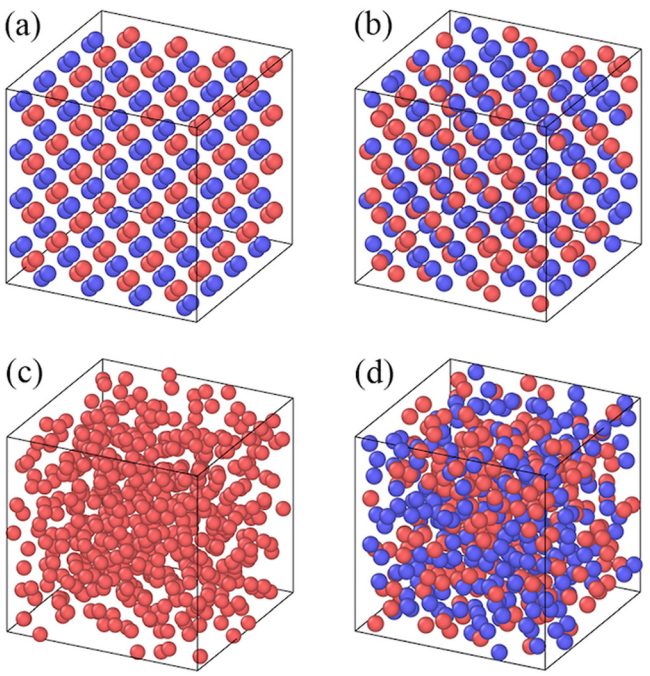

FIG. 1. Model structures: (a) o-SiGe, (b) d-SiGe, (c) a-Si, and (d) a-SiGe. The a-Ge structure is not shown as it is essentially topologically identical to a-Si structure. The red atoms are Si and the blue atoms are Ge.

where V is the system volume, k_B is the Boltzmann constant, T is the system temperature, and the angular brackets denote an average over simulation time. In each case, we executed 5 independent simulation runs for the perfectly ordered structure for each size, and 3 to 5 runs for independent configurations for amorphous and disordered structures for each size to assess the statistical error. To obtain a reliably well-converged value of κ, relatively long integration times (up to 200 ps) were required. We use the Fast Fourier Transform (FFT) method[23] to compute the autocorrelation function efficiently. All our MD simulations were performed using the LAMMPS package[24] with a time step of 0.5 fs.

C. Phonon lifetime determination

To gain a deeper understanding of the thermal transport in various structures described above, we carried out dynamical structure factor calculations within the framework of equilibrium MD (EMD)[25,26] that allow us to determine the lifetime of individual phonons. The longitudinal and transverse structure factors, $S_L(\boldsymbol{k}, \omega)$ and $S_T(\boldsymbol{k}, \omega)$, respectively, for a given wave vector $\boldsymbol{k}$ are given as

$$S_\alpha(\boldsymbol{k},\omega) = \frac{\boldsymbol{k}^2}{2\pi\omega^2 N}\int \langle \boldsymbol{j}_\alpha(\boldsymbol{k},t)\cdot\boldsymbol{j}_\alpha(-\boldsymbol{k},0)\rangle \exp(i\omega t)dt, \quad (2)$$

where α is L or T and N is the number of atoms in the simulation cell and

$$\boldsymbol{j}_L(\boldsymbol{k},t) = \sum \left(\boldsymbol{v}_i(t)\cdot\hat{\boldsymbol{k}}\right)\hat{\boldsymbol{k}}\exp(i\boldsymbol{k}\cdot\boldsymbol{r}_i(t)), \quad (3)$$

$$\boldsymbol{j}_T(\boldsymbol{k},t) = \sum \left(\boldsymbol{v}_i(t) - \left(\boldsymbol{v}_i(t)\cdot\hat{\boldsymbol{k}}\right)\hat{\boldsymbol{k}}\right)\exp(i\boldsymbol{k}\cdot\boldsymbol{r}_i(t)), \quad (4)$$

where $\hat{\boldsymbol{k}} = \boldsymbol{k}/|\boldsymbol{k}|$, $\boldsymbol{v}_i$, and $\boldsymbol{r}_i$ refer to the velocity and equilibrium position of the ith atom, and the summation over all the atoms in the simulation cell.

The structure factor peak can be fitted by the Lorentz function as

$$S_\alpha(\boldsymbol{k},\omega) = \frac{C_0(\boldsymbol{k})}{\left[\Omega_\alpha(\boldsymbol{k}) - \omega\right]^2 + \Gamma_\alpha^2(\boldsymbol{k})}, \quad (5)$$

where we have introduced the mode frequencies $\Omega_\alpha(\boldsymbol{k})$ and half-linewidths $\Gamma_\alpha(\boldsymbol{k})$. Here $C_0(\boldsymbol{k})$ is a mode related constant. Phonon lifetime can be evaluated from the fitted half-linewidth $\Gamma_\alpha(\boldsymbol{k})$ as

$$\tau(\omega) = \frac{1}{2\Gamma_\alpha(\omega)}. \quad (6)$$

III. RESULTS AND DISCUSSION

A. Thermal conductivity

To address possible size effects, we determined thermal conductivity as a function of the simulation cell size. The results are shown in Fig. 2 where we plot the inverse of thermal conductivities, $1/\kappa$, as a function of inverse of the side length of the simulation cells, $1/L$.

In the case of o-SiGe (Fig. 2, top panel), we observe some system-size dependence that may be systematic, but

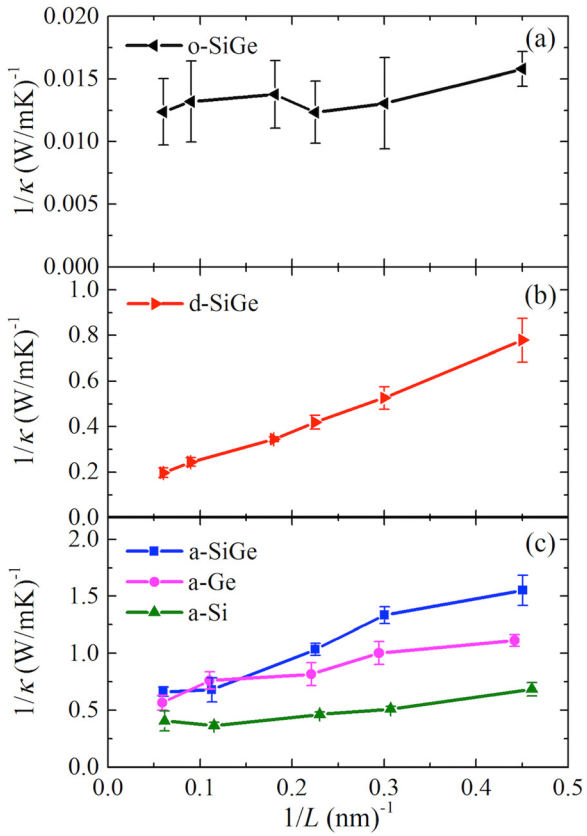

FIG. 2. The inverse of thermal conductivity as a function of the inverse of sample size for o-SiGe, d-SiGe, a-SiGe, a-Ge, and a-Si. There is a clear system-size dependence for d-SiGe and amorphous structures. The thermal conductivities of amorphous structures are much lower than that of d-SiGe, implying stronger scattering from structural disorder than compositional disorder.

can also be attributed to the statistical fluctuations, which is consistent with the results obtained for crystalline silicon.[27,28] From Fig. 2, we estimate the bulk thermal conductivity of o-SiGe to be 80 W/mK. For reference, we note that the bulk thermal conductivity of crystalline silicon and germanium determined by equilibrium MD (EMD) calculation and using the same potential was reported to be 197 W/mK and 70 W/mK, respectively.[9]

In the case of d-SiGe (Fig. 2, middle panel), there is a strong and systematic system-size dependence of thermal conductivity, with larger structures characterized by larger thermal conductivity. Since with increasing size phonons with larger wavelength and lower frequency are introduced, this result indicates that low frequency phonons have a relatively larger contribution to thermal conductivity than in the case of o-SiGe. By extrapolating to the infinite size, we estimate the d-SiGe conductivity to be 8.6 W/mK, which is in good agreement with prior work using the same potential and methodology[9] as well as with experimental results.[10,11] We note that in the case of LJ alloys, the size dependence is essentially non-existent;[16] this can be attributed to large anharmonicity which drastically reduces the lifetime of the low frequency phonons, and thus their contribution to overall thermal conductivity.

The thermal conductivity value of 8.6 W/mK for d-SiGe is about eight times larger than the one obtained from non-equilibrium MD (NEMD) simulations[12] using the Stillinger–Weber potential and three times larger than that obtained from the approach-to-equilibrium MD (AEMD) simulations[14] using the same Tersoff potential. We attribute these lower thermal conductivity predictions obtained by NEMD difficulties with proper assessment on the strong system size effects exhibited by NEMD and AEMD simulations, which are particularly pronounced for SiGe alloys.

The large reduction in conductivity by random alloying is a direct consequence of the enhanced phonon scattering from compositional disorder. Such scattering is particularly effective for short and medium wavelength phonons (see our phonon lifetime analysis below), while it is less effective for the long-wavelength phonons. This perhaps explains why the size effects are much more pronounced for d-SiGe than for o-SiGe.

For amorphous structures (Fig. 2, bottom panel), there is also a clear system-size dependence, however, not that strong as in the case of d-SiGe. Furthermore, conductivities are significantly lower than those characterizing the disordered structure. The thermal conductivities of a-Si and a-Ge are estimated to be 2.9 W/mK and 1.8 W/mK, respectively. In particular, the bulk thermal conductivity of a-SiGe is estimated to be 1.6 W/mK, which is about 5 times lower than the d-SiGe value. Similar as in the case d-SiGe, our EMD result predicts a-SiGe thermal conductivity twice larger as that obtained by AEMD simulations[14] using the same potential.

The much lower thermal conductivities of a-Si and a-Ge compared to d-SiGe implies that the pure structural disorder present in single component amorphous semiconductor structures scatters phonons more effectively than the pure compositional disorder, an effect also observed in LJ alloys.[16,17] Furthermore, the thermal conductivity of a-SiGe is within the range bound by thermal conductivities of pure a-Si and pure a-Ge, indicating that the heat transport in a-Si and a-Ge is already limited by the structural disorder, and the introduction of the compositional disorder does not reduce it any further. Finally, we notice that the conductivities of amorphous structures converge for large system sizes faster than in the case of disordered alloys, consistent with more effective low frequency phonon scattering.

B. Phonon lifetime analysis

To identify more directly the reason for the system-size dependence, we evaluated the phonon lifetimes for three SiGe alloy structures using the method described in Sec. II C. A sample fit for $\boldsymbol{k} = \frac{1}{30} \cdot \frac{2\pi}{a}[100]$ is shown in Fig. 3.

Such computed phonon lifetimes are plotted in Fig. 4 for o-SiGe, d-SiGe, and a-SiGe structures containing 216 000 atoms each. At high frequency ($\nu > 1.5$ THz), the lifetime of both longitudinal and transverse modes for d-SiGe and a-SiGe scale as ω^{-4}, suggesting a Rayleigh scattering mechanism arising from the atomic-level compositional or structural disorder.[29] The predicted lifetimes for a-SiGe in this region are similar to those observed by He *et al.*[30] for a-Si using the same Tersoff potential. At a low frequency ($\nu < 1.5$ THz), the lifetimes of longitudinal and transverse

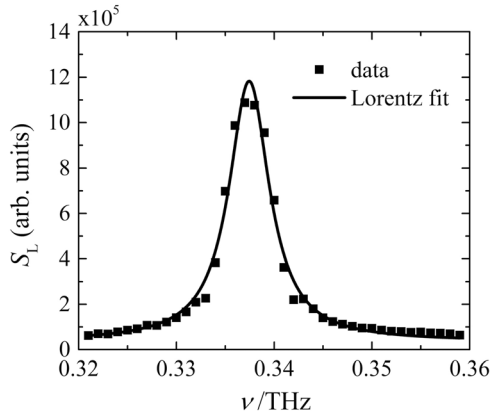

FIG. 3. The dynamical structure factor data were fitted by the Lorentz function to obtain resonance frequency and half-linewidth.

modes for d-SiGe and a-SiGe show an approximate ω^{-2} and ω^{-1} dependence, respectively, which suggests an Umklapp phonon-phonon scattering mechanism.[31] A previous study of Lennard–Jones alloy with the same mass disorder as d-SiGe exhibited a similar trend for phonon lifetimes;[32] however, Refs. 16 and 17 indicate that the phonon lifetimes scale as ω^{-4} at intermediate frequencies and ω^{-2} at higher frequencies in LJ alloys.

We note that the relatively long phonon lifetimes ($\sim$1 ns) and the long wavelength comparable to the system size at low frequency make the associated error in lifetime determination rather large and this is perhaps responsible for a relatively large scatter in the data in the low frequency range.

For d-SiGe, the lifetimes of the low-frequency modes are quite high, of the order of 100 ps. Consequently, a large fraction of thermal conductivity is expected to originate from low frequency modes. Similar observations were reported for d-SiGe by Garg *et al.*[4] using a first principles-based approach, demonstrating that 65% of the heat in d-SiGe is conducted by phonons of frequency less than 1 THz at 300 K. By contrast to disordered structures, for ordered structures (such as o-SiGe), high-frequency modes have much larger lifetimes, and thus contribute much more to the overall much larger thermal conductivity, rendering size effects associated with low-frequency phonon contributions much less pronounced (see Fig. 2). Also, this size dependence observed in simulations is consistent with the frequency dependence of thermal conductivity of d-SiGe and a-Si observed in experiments.[10,33]

We also note that the overall phonon lifetimes for a-SiGe are significantly shorter than those for d-SiGe, with the most pronounced difference in the low frequency range. This suggests that the structural disorder results in stronger phonon-phonon scattering, causing a further reduction of thermal conductivity compared to a purely compositional disorder, and explaining the fact that size dependence for amorphous structures is less pronounced than that which characterizes disordered crystalline alloys. The same behavior was observed for LJ alloys[16,17] underlying the generality of this observation. Furthermore, Fig. 4 shows that the difference in lifetimes between amorphous and disordered alloys is much more pronounced for transverse modes than longitudinal modes. We will discuss this issue later in the article in the context of elastic heterogeneities and temperature dependence.

C. Local property analysis

To shed further light on the relative role of compositional and structural disorder, we analyzed distributions of local density and local elastic constant. The spatial mass fluctuation is firmly related to the wave scattering in the disordered materials, as measured experimentally by small-angle X-ray scattering.[34] To determine the distributions, we divided the original simulation cell of side length $L = 30a$ into smaller cubic domains with a linear size $D = Na\,(1 \leq N \leq 4)$. In the calculation of local properties, we associated each atom with an atomic volume cube and in cases where the atom was near the edge of the domain, its contribution to local properties was partially assigned to the adjacent domains weighted by the volume of the cube overlapping with a given domain.

The probability distribution of local mass densities for $D = a$ case (average of 8 atoms per domain) is shown in Fig. 5(a). d-SiGe and a-SiGe have very similar distributions indicating that the mass fluctuation cannot explain differences in the thermal conductivities in the two structures.

Next, we examined distributions of local elastic properties, as they affect the thermal properties of disordered materials.[35] The local elastic constant (shear modulus in this case) was determined by a simple shear deformation. The atomic level stress was obtained by the virial formula and subtraction of the atomic-level stress in the undeformed state from the deformed state. In one deformation type we did not allow the structure to relax, thus imposing a homogeneous strain, resulting in an "unrelaxed" shear modulus. The "relaxed" shear

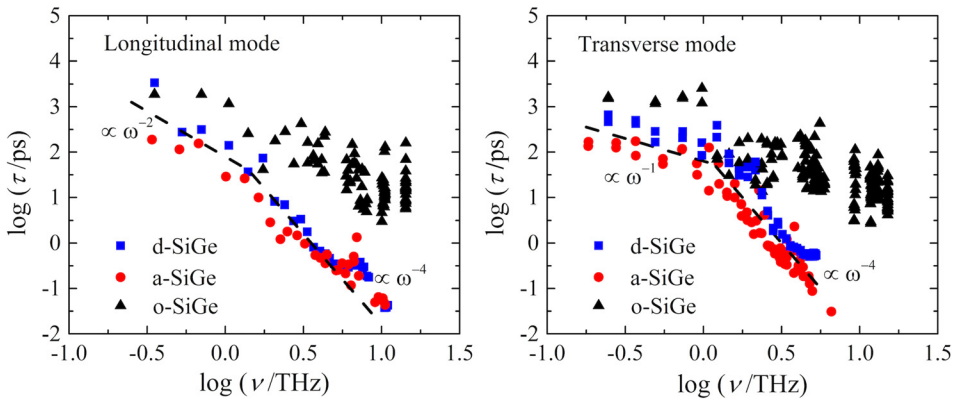

FIG. 4. Phonon lifetimes obtained from structure factor calculations for o-SiGe, d-SiGe, and a-SiGe. At high frequency, both longitudinal and transverse modes for d-SiGe and a-SiGe show a ω^{-4} scaling. At low frequency, there is a ω^{-2} scaling for longitudinal modes and a ω^{-1} scaling for transverse modes.

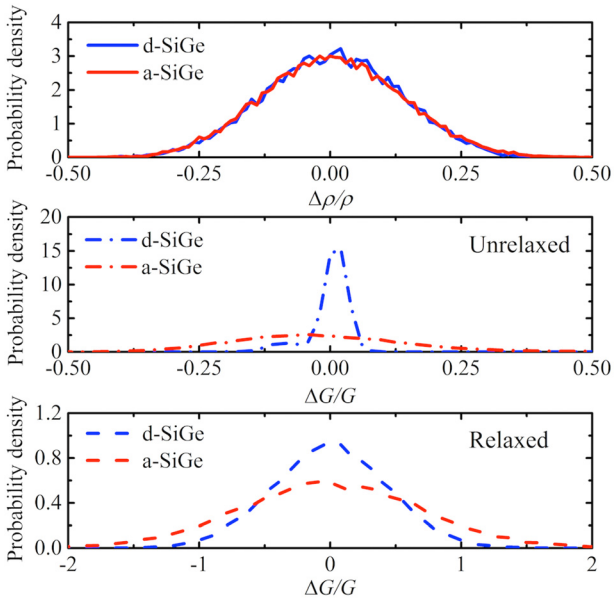

FIG. 5. Probability distribution function of (a) local mass densities ρ, (b) local unrelaxed shear modulus G, and (c) local relaxed shear modulus G of d-SiGe and a-SiGe for domains size $D = a$.

modulus was evaluated from atomic stresses after relaxation. In this case, the local strain was not homogeneous, and evaluated by the procedure described in Ref. 36.

The local unrelaxed shear modulus distributions calculated for domains with $D = a$ are shown in Fig. 5(b). a-SiGe has a 4 times broader distribution of the local unrelaxed shear modulus than d-SiGe. After the relaxation [see Fig. 5(c)], the distributions of the local shear modulus, G, become broader, while contrast between two structures is still significant. Evaluation of the local mass and modulus fluctuations for larger domain sizes results in narrowing the distributions, but the ratios of the distribution widths remain largely unchanged. This analysis indicates that elastic heterogeneity associated with an amorphous structure is a key factor responsible for strong scattering of low frequency phonons.

We also analyzed the fluctuations of C_{11} elastic constant (not shown) and observed similar behavior as in the case of shear modulus, G. However, the width of the normalized fluctuations ($\Delta G/G$ and $\Delta C_{11}/C_{11}$) is about twice larger in the case of shear modulus. Since shear modulus relates to transverse modes and C_{11} relates to longitudinal modes, one can speculate that more significant differences between disordered and amorphous structures for transverse mode lifetimes (see Fig. 4) are associated with large local shear modulus fluctuations.

D. Temperature dependence

Finally, we investigated the temperature dependence of conductivity, that is expected to be significant, even for disordered SiGe alloys, since low frequency phonons and associated Umklapp scattering play important roles in thermal conductivity of these highly harmonic materials. We calculated the thermal conductivities using the same procedure as described in Sec. II B at temperatures: 100 K, 300 K, 500 K, and 1000 K.

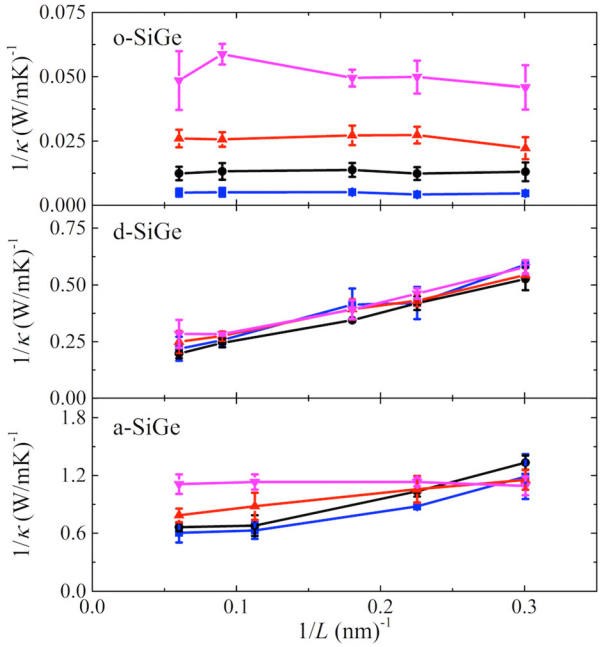

FIG. 6. The inverse of thermal conductivity as a function of the inverse of sample size for o-SiGe, d-SiGe, and a-SiGe at different temperatures: 100 K (blue squares), 300 K (black circles), 500 K (red upper triangles), and 1000 K (magenta inverted triangles). There is a minor system size dependence in o-SiGe and a strong size dependence in d-SiGe at all temperatures, while the size effect diminishes as the temperature increases in a-SiGe.

The inverse thermal conductivity as a function of the inverse of the system size is shown in Fig. 6. The ordered structure (o-SiGe), as observed before, exhibits minor system size effects at all temperatures studied. By contrast, significant system size effects in d-SiGe are observed at all temperatures. In the case of a-SiGe, the system size dependence gradually declines when the temperature increases, suggesting that the contribution of the low-frequency phonons to the thermal conductivity is depressed at a high temperature.

The extrapolated bulk thermal conductivities as a function of temperature are shown in Fig. 7. As temperature

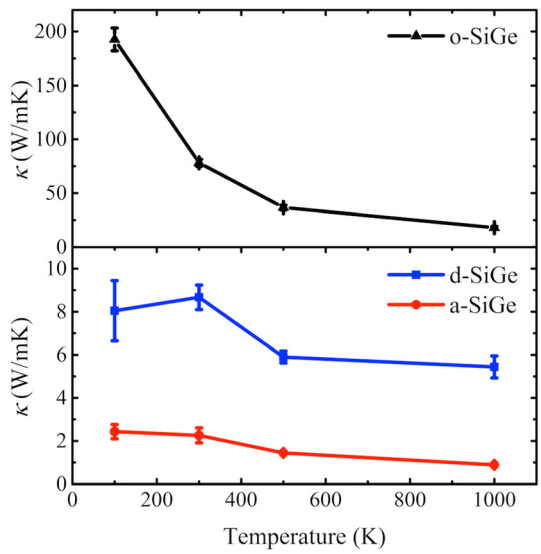

FIG. 7. The thermal conductivity decreases as the temperatures increases for o-SiGe, d-SiGe, and a-SiGe.

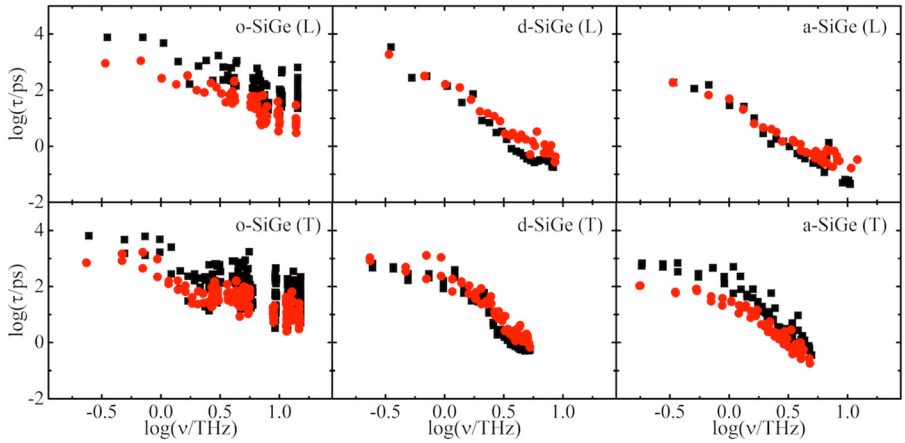

FIG. 8. Phonon lifetimes for o-SiGe, d-SiGe, and a-SiGe at 300 K (black squares) and 1000 K (red circles). At a high temperature, the phonon lifetimes decrease in o-SiGe, while they remain the same in d-SiGe. For a-SiGe, the longitudinal modes are not affected by temperature, while the transverse modes have a lower lifetime at a high temperature.

increases, the thermal conductivity generally decreases for all three SiGe alloy models. In the case of d-SiGe, it appears that conductivity increases between 100 K and 300 K. However, considering the statistical errors (see Fig. 7), we are not confident that this observation is significant. The most pronounced decrease is observed for o-SiGe which is characteristic of the Umklapp phonon-phonon scattering mechanisms across the whole phonon spectrum, which leads to the trend of $\kappa \propto \frac{1}{T}$.[37] In the case of the disordered structures, the decrease is less pronounced, since structural phonon scattering is dominant here. Nevertheless, the conductivity decrease with increasing temperature is still clear, particularly for the amorphous structure, indicating that phonon-phonon scattering plays a significant role for disordered SiGe structures.

To gain further understanding into this temperature dependence, we calculated the phonon lifetimes for o-SiGe, d-SiGe, and a-SiGe at 1000 K, and compared them with those at 300 K. In the case of o-SiGe, the phonon lifetimes of both longitudinal and transverse modes decrease significantly and uniformly across the whole frequency range at high temperature (see Fig. 8), which is characteristic of all phonons exhibiting the phonon-phonon scattering mechanism. By contrast, essentially all phonon lifetimes for d-SiGe are weakly affected by temperature, leading to rather weak thermal conductivity dependence on temperature (see Fig. 7).

The case of a-SiGe is perhaps the most interesting. According to Fig. 8 the lifetimes of longitudinal modes are not significantly affected by temperature, but the lifetimes of transverse modes decrease at high temperature especially at the low frequency regime. This suggests that effective anharmonicity exhibited by transverse modes is more pronounced than for longitudinal modes. The reason for the different responses of longitudinal and transverse modes in a-SiGe is quite unclear to us, and needs more work in the future.

IV. CONCLUSIONS

In summary, we investigated thermal conductivity and phonon lifetimes in relation to structural characteristics such as local densities and local elastic constants and to temperature in several SiGe alloy structures by means of EMD simulations. Our studies demonstrated that in the case of disordered and amorphous semiconducting alloys in the high frequency range, the phonons exhibit Rayleigh scattering caused by compositional and/or structural disorder, respectively. Below ~1.5 THz, the Umklapp phonon-phonon scattering mechanism dominates. We also observed that structural scattering is significantly stronger than compositional scattering, resulting in a-SiGe thermal conductivity being about 5 times lower than that of d-SiGe, but within the range bound by thermal conductivities of pure a-Si and pure a-Ge. This observation indicates that alloying by itself is unlikely to be a fruitful strategy to reduce the thermal conductivity of amorphous materials. Furthermore, we revealed that the stronger scattering in a-SiGe is attributed to the higher level of elastic heterogeneity caused by structural disorder. The temperature dependence of thermal conductivity indicated the importance of the Umklapp phonon-phonon scattering in thermal conductivity of SiGe alloys. Comparison between phonon lifetimes for disordered and amorphous alloys and temperature effect studies demonstrated a marked difference in response to transverse and longitudinal modes of disorder and temperature.

Our results also emphasize the importance of proper account of the size effects in thermal conductivity determination, even when using equilibrium molecular dynamics and periodic boundary conditions. Contrary to the intuition based on the low thermal conductivity values, the size effects can be particularly significant in this case of some disordered materials,[31] that are characterized by a low degree of anharmonicity.

ACKNOWLEDGMENTS

This work was supported by the New York State NYSTAR funded Focus Interconnect Center.

[1]G. A. Slack and M. A. Hussain, J. Appl. Phys. **70**, 2694 (1991).
[2]D. R. Clarke and S. Phillpot, Mater. Today **8**, 22 (2005).
[3]M. C. Steele and F. D. Rosi, J. Appl. Phys. **29**, 1517 (1958).
[4]J. Garg, N. Bonini, B. Kozinsky, and N. Marzari, Phys. Rev. Lett. **106**, 045901 (2011).
[5]L. Yin, E. Kyung Lee, J. Woon Lee, D. Whang, B. Lyong Choi, and C. Yu, Appl. Phys. Lett. **101**, 043114 (2012).
[6]Y. He, D. Donadio, and G. Galli, Nano Lett. **11**, 3608 (2011).
[7]X. Li and R. Yang, J. Appl. Phys. **113**, 104306 (2013).
[8]S. Volz, J. B. Saulnier, G. Chen, and P. Beauchamp, Microelectron. J. **31**, 815 (2000).
[9]Y. He, I. Savić, D. Donadio, and G. Galli, Phys. Chem. Chem. Phys. **14**, 16209 (2012).
[10]Y. Koh and D. Cahill, Phys. Rev. B **76**, 075207 (2007).

[11]B. Abeles, Phys. Rev. **131**, 1906 (1963).
[12]A. Skye and P. K. Schelling, J. Appl. Phys. **103**, 113524 (2008).
[13]M. Upadhyaya, S. N. Khatami, and Z. Aksamija, J. Mater. **30**, 2649 (2015).
[14]K. R. Hahn, C. Melis, and L. Colombo, Eur. Phys. J. B **87**, 150 (2014).
[15]H. Mizuno, S. Mossa, and J.-L. Barrat, Sci. Rep. **5**, 14116 (2015).
[16]H. Mizuno, S. Mossa, and J.-L. Barrat, Phys. Rev. B **94**, 144303 (2016).
[17]H. Mizuno, S. Mossa, and J. L. Barrat, Proc. Natl. Acad. Sci. U.S.A. **111**, 11949 (2014).
[18]J. Z. Tischler, J. D. Budai, D. E. Jesson, G. Eres, and P. Zschack, Phys. Rev. B **51**, 10947 (1995).
[19]M. Ishimaru, S. Munetoh, and T. Motooka, Phys. Rev. B **56**, 15133 (1997).
[20]J. Tersoff, Phys. Rev. B **39**, 5566 (1989).
[21]O. Madelung, M. Schulz, and H. Weiss, *Physics of Group IV Elements and III-V Compounds* (Springer-Verlag, Berlin, 1995).
[22]W. G. Hoover, *Computational Statistical Mechanics* (Elsevier, Amsterdam, 1991).
[23]J. W. Cooley and J. W. Tukey, Math. Comput. **19**, 297 (1965).
[24]S. Plimpton, J. Comput. Phys. **117**, 1 (1995).
[25]H. Shintani and H. Tanaka, Nat. Mater. **7**, 870 (2008).
[26]J. M. Larkin and A. J. H. McGaughey, Phys. Rev. B **14**, 144303 (2013).
[27]D. P. Sellan, E. S. Landry, J. E. Turney, A. J. H. McGaughey, and C. H. Amon, Phys. Rev. B **81**, 214305 (2010).
[28]S. Volz and G. Chen, Phys. Rev. B **61**, 2651 (2000).
[29]R. C. Zeller and R. O. Pohl, Phys. Rev. B **4**, 2029 (1971).
[30]Y. He, D. Donadio, and G. Galli, Appl. Phys. Lett. **98**, 144101 (2011).
[31]C. Herring, Phys. Rev. **95**, 954 (1954).
[32]J. M. Larkin and A. J. H. McGaughey, J. Appl. Phys. **114**, 023507 (2013).
[33]H.-S. Yang, D. G. Cahill, X. Liu, J. L. Feldman, R. S. Crandall, B. A. Sperling, and J. R. Abelson, Phys. Rev. B **81**, 104203 (2010).
[34]C. Levelut, A. Faivre, R. Le Parc, B. Champagnon, J. L. Hazemann, L. David, C. Rochas, and J. P. Simon, J. Non-Cryst. Solids **307–310**, 426 (2002).
[35]H. Mizuno, S. Mossa, and J.-L. Barrat, Europhys. Lett. **104**, 56001 (2013).
[36]F. Shimizu, S. Ogata, and J. Li, Mater. Trans. **48**, 2923 (2007).
[37]J. M. Ziman, *Electrons and Phonons* (Oxford University Press, Oxford, 1960).